Preferentially adsorbed layer on the Zn surface manipulating ion distribution for stable Zn metal anodes

*Qiang Guo**[,1], *Gele Teri*[1], *Weixing Mo*[2], *Jianhang Huang*[3], *Feng Liu**[, 2], *Minghui Ye**[, 4], *Dawei Fu*[1]

1 Institute for Science and Applications of Molecular Ferroelectrics, Key Laboratory of the Ministry of Education for Advanced Catalysis Materials, Zhejiang Normal University, Jinhua, Zhejiang 321004 China

2 State Key Laboratory of Nonlinear Mechanics, Institute of Mechanics, Chinese Academy of Sciences, Beijing 100190, P. R. China

3 Key Laboratory of the Ministry of Education for Advanced Catalysis Materials, College of Chemistry and Materials Science, Zhejiang Normal University, Jinhua, 321004 China

4 School of Chemical Engineering and Light Industry, Guangdong University of Technology, Guangzhou 510006, P. R. China

AUTHOR INFORMATION

Corresponding Author

qiangguo@zjnu.edu.cn; liufeng@imech.ac.cn; mhye@gdut.edu.cn

Experimental section

Electrolyte preparation: 2.88 g of $ZnSO_4 \cdot 7H_2O$ was mixed with 5 mL of deionized water to obtain the 2 M $ZnSO_4$ solution. Then, 5 wt % butyrolactam (0.394 g) was

added into 2M $ZnSO_4$ solution.

Material characterization: X-ray powder diffraction (XRD) patterns were performed on a D8 Focus diffractometer (Bruker) with Cu-Kα radiation (λ=0.15405 nm). The morphology of zinc electrodes was investigated by scanning electron microscopy (SEM, SUPRA 55) and atomic force microscopy (AFM, Brucker Bioscope Resolve, Germany). X-ray photoelectron spectroscopy (XPS) analysis was carried out by employing a Thermo Fisher-Escalab 250Xi equipped with Al Kα radiation. The information of functional groups was characterized by a Fourier transform infrared spectrometer (FTIR, Nicolet NEXUS 670). Nuclear magnetic resonance (NMR) spectra were recorded on a Bruker Advance III 400 M NMR spectrometer. 90 μL of electrolytes with different amounts of BA additives was added into 500 μL of DMSO for the electrolyte characterization.

Electrochemical Measurements: The CR2025-type Zn symmetric cells were assembled with polished Zn plates, prepared electrolytes and glass fiber separators. Zn-Cu half cells were fabricated by using polished Zn plates, Cu foils, and glass fiber separators. Cyclic voltammetry (CV), linear sweep voltammetry (LSV), chronoamperometry (CA) curves were measured on a CHI 760E electrochemical workstation. Electrochemical impedance spectroscopy (EIS) data were collected in the frequency range of 0.01 Hz to 100 k Hz with an AC voltage of 10 mV. Galvanostatic charge/discharge (GCD) curves were conducted using a battery test system (LAND CT2001A, China). I_2-based composite cathode was prepared by our previously reported work.[1] I_2-based composite/V_2O_5, acetylene black and PVDF were uniformly mixed in a mass ratio of

7:2:1.

DFT Calculations: All the density functional theory (DFT) calculations were estimated based on the Vienna Ab initio Simulation Package (VASP).[2] The generalized gradient approximation (GGA) with the exchange-correlation functional Perdew-Burke-Ernzerhof (PBE)[3] was carried out. The plane wave basis set is used with cutoff energy of 400 eV and the energy convergence of 10^{-4} eV. The precision of the geometry structure optimization with forces on atoms was small than 0.01eV/Å. Moreover, the diffusion behavior of Zn on the Zn (101) surface was calculated by the Nudged Elastic Band (NEB)[4] method. For the adsorption process of H_2O and BA molecules on Zn (101) facet was described by equation (1), i.e.

$$E_{adsorption} = E_{adsorbate} + E_{slab} - E_{adsorbate\text{ - }slab}, \#(1)$$

where $E_{adsorbate\text{ - }slab}$ and E_{slab} were the total energy of the optimized electrode surface with and without the adsorbate, and $E_{adsorbate}$ was the total energy of the adsorbate.

For the migration energy of Zn on the Zn (101) surface was calculated by equation (2), i.e.

$$E_{relative} = E_{final} - E_{initial}, \#(2)$$

where E_{final} and $E_{initial}$ were the total energies of final state and initial state, respective. All the energies were obtained directly from DFT calculations.

MD Simulation: LAMMPS (Large-scale Atomic/Molecular Massively Parallel Simulator)[5] was employed to study the solvation structure of 2 M $ZnSO_4$ with and without BA molecules. The simulation calculation was conducted with a time step of 0.1 fs. The cutoff radius was 1 nm for both Lennard-Jones interactions and Coulomb

interactions. To be specific, SPC water model[6] was applied to descript interaction between water molecules, while Coulomb potential and Lennard-Jones potential were used to describe the interaction between water molecule and ion atoms. For Zn^{2+} ($\varepsilon = 0.0019\ eV$, $\sigma = 2.593$ Å), SO_4^{2-} (S: $\varepsilon = 0.0108\ eV$ and $\sigma = 3.55$ Å, O: $\varepsilon = 0.0087\ eV$ and $\sigma = 3.65$ Å) and PI (C: $\varepsilon = 0.0072\ eV$ and $\sigma = 3.4$ Å, N: $\varepsilon = 0.0068\ eV$ and $\sigma = 3.226$ Å, O: $\varepsilon = 0.0067\ eV$ and $\sigma = 3.166$ Å, H: $\varepsilon = 0.0\ eV$ and $\sigma = 0.0$ Å), these parameters are well fitted with the existing potential function. [7, 8] All charge settings are shown in Fig.1e. Periodic boundary conditions were applied in all three directions. Energy minimization was conducted to gain a stable state for liquid systems. The size of the simulation box was 8 nm × 8 nm × 8 nm. In our simulations, NPT ensemble was chosen, zero pressure and 300 K were set, and the total relaxation time was 100 ps. Equilibrium properties like the radial distribution functions (RDFs) and the coordination numbers could be computed according to the simulation results, where RDFs describes how density varies as a function of distance from a reference particle.

Electric field distribution calculation details: Finite element method was applied to solve Poisson's equation to show the electric field amplitude's distribution of the rough surface.

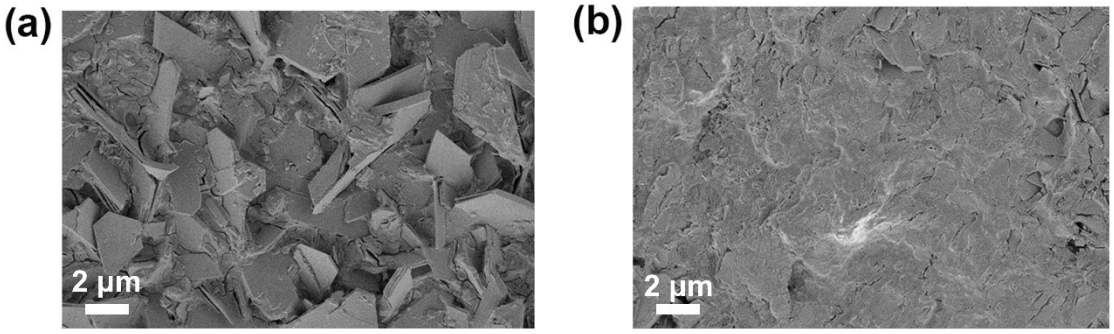

Figure S1. SEM images of Zn foils immersed in (a) ZSO-H_2O and (b) ZSO-H_2O-BA electrolytes after 7 days.

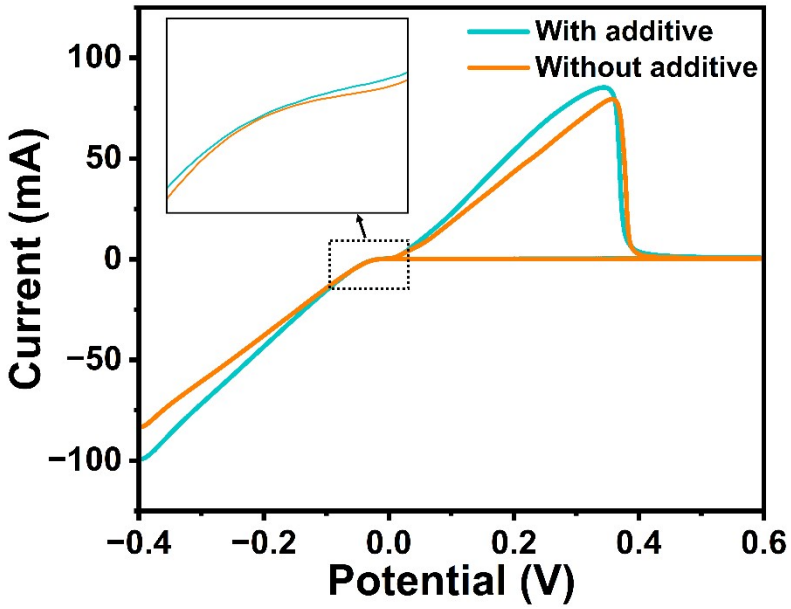

Figure S2. CV curves of Zn-Ti half cells in ZSO-H_2O and ZSO-H_2O-BA electrolytes at 2 mV/s.

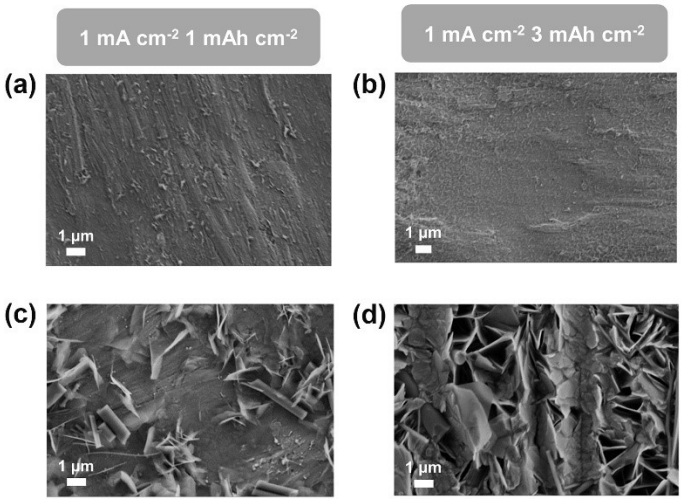

Figure S3. SEM images of Zn deposits on Cu foil after plating with a capacity of a) 1, and b) 3 mAh cm^{-2} in (a and b) ZSO-H_2O-BA and (c and d) ZSO-H_2O electrolytes.

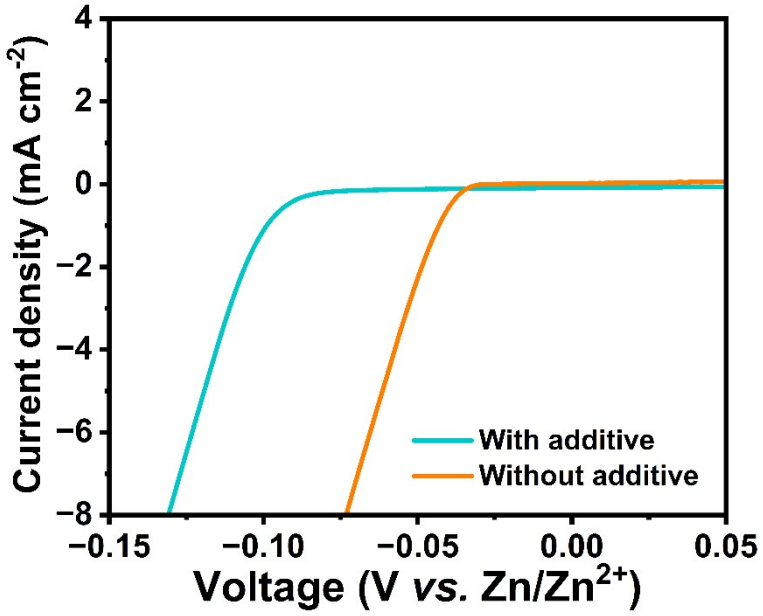

Figure S4. LSV curves of the Zn electrodes at 2 mV/s.

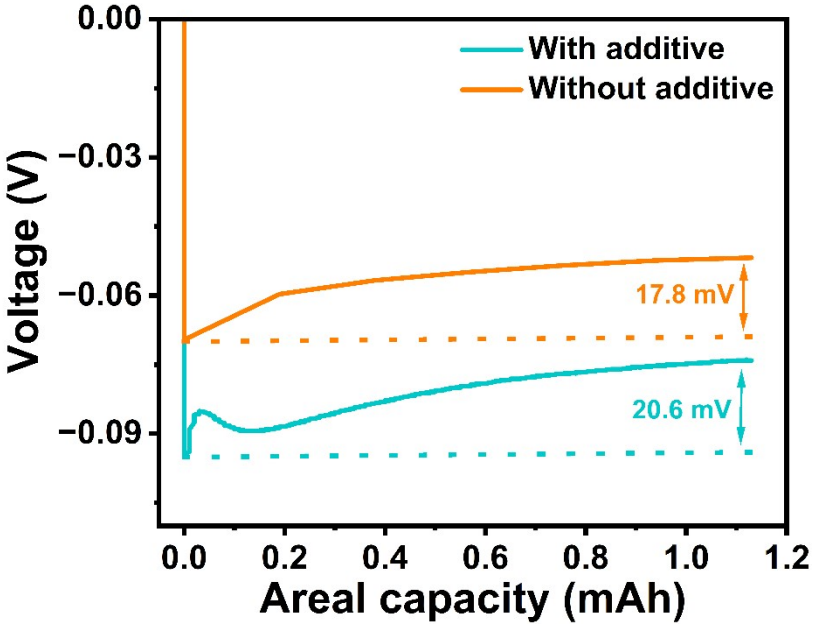

Figure S5. (i) Nucleation overpotential of the Zn-Zn symmetric cells a current density of 10 mA cm^{-2}.

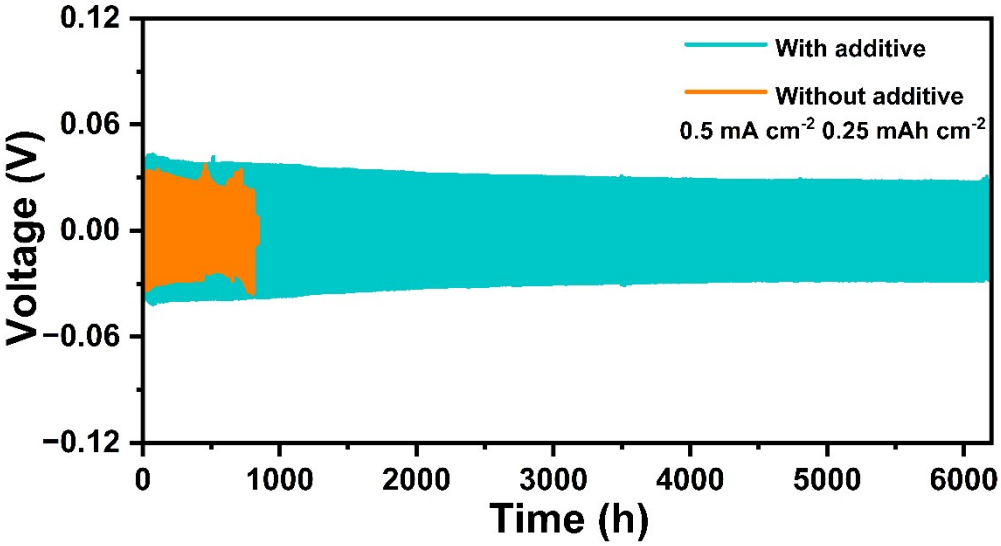

Figure S6. Long-term cycling stability of Zn-Zn symmetric cells at 0.5 mA cm^{-2}.

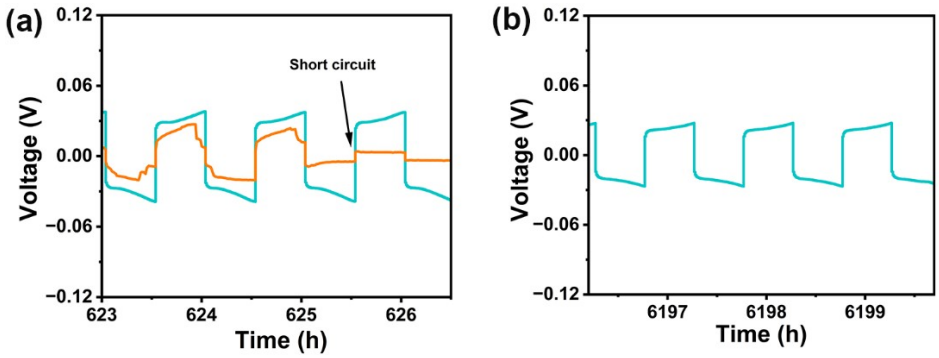

Figure S7. Amplified voltage curves at 0.5 mA cm^{-2} and 0.25 mAh cm^{-2}.

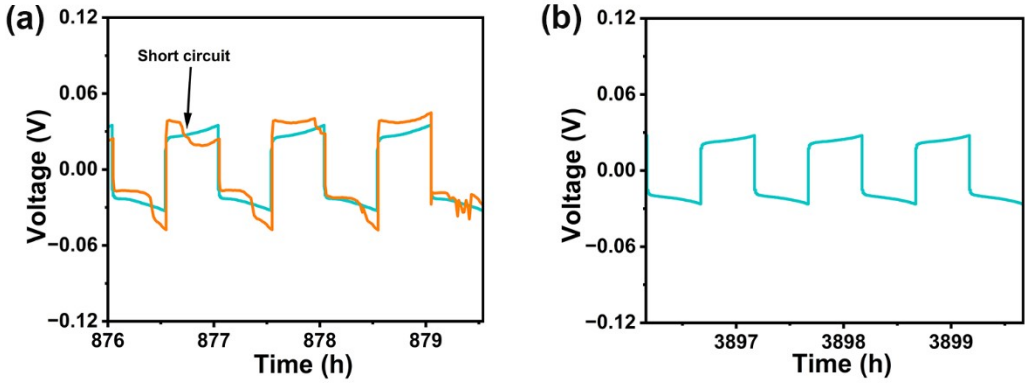

Figure S8. Amplified voltage curves at 1 mA cm^{-2} and 0. 5 mAh cm^{-2}.

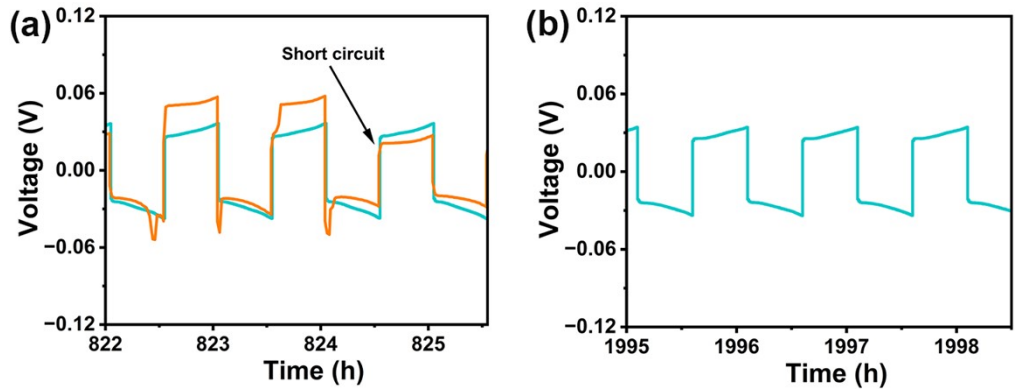

Figure S9. Amplified voltage curves at 2 mA cm^{-2} and 1 mAh cm^{-2}.

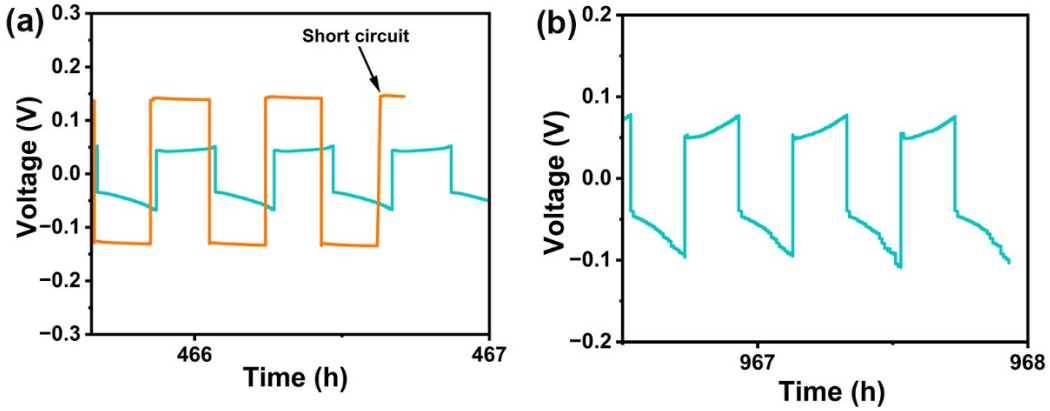

Figure S10. Amplified voltage curves at 5 mA cm^{-2} and 1 mAh cm^{-2}.

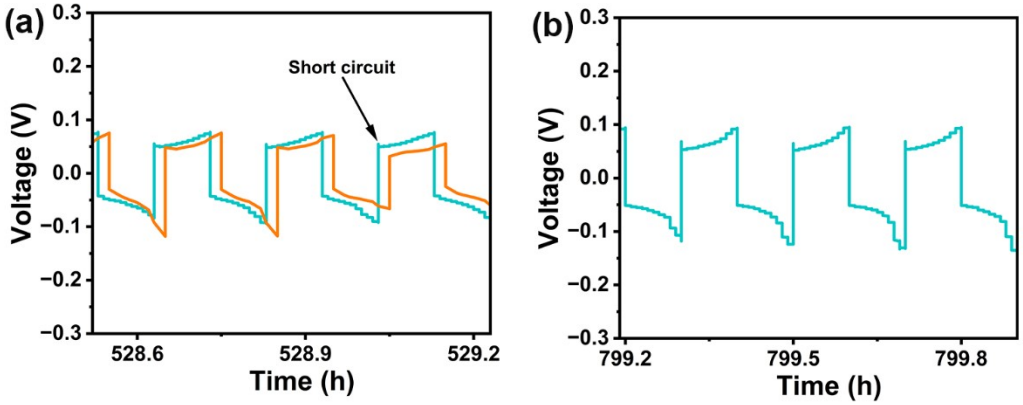

Figure S11. Amplified voltage curves at 10 mA cm^{-2} and 1 mAh cm^{-2}.

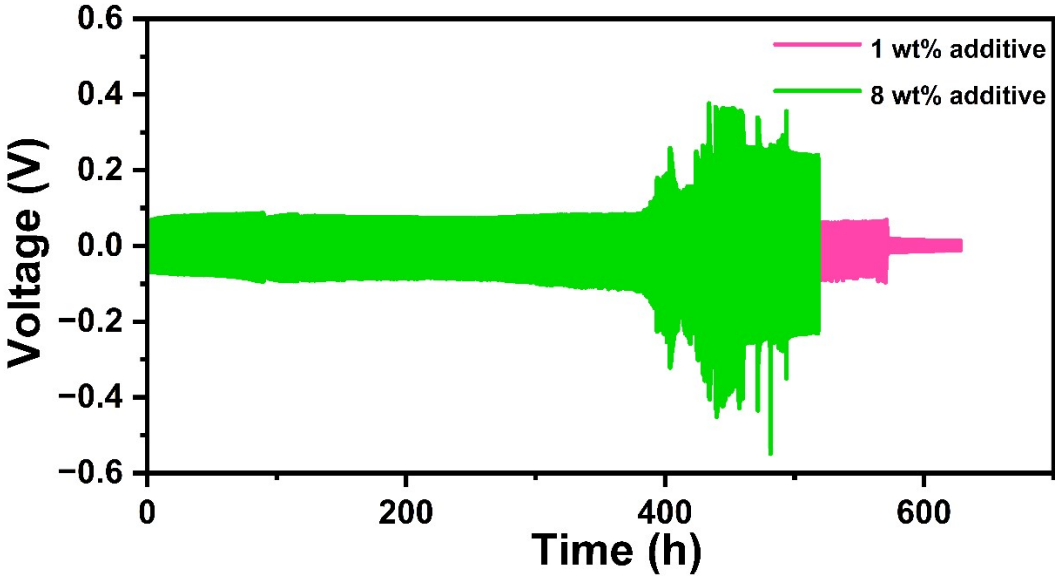

Figure S12. Amplified voltage curves at 5 mA cm^{-2} and 1 mAh cm^{-2}.

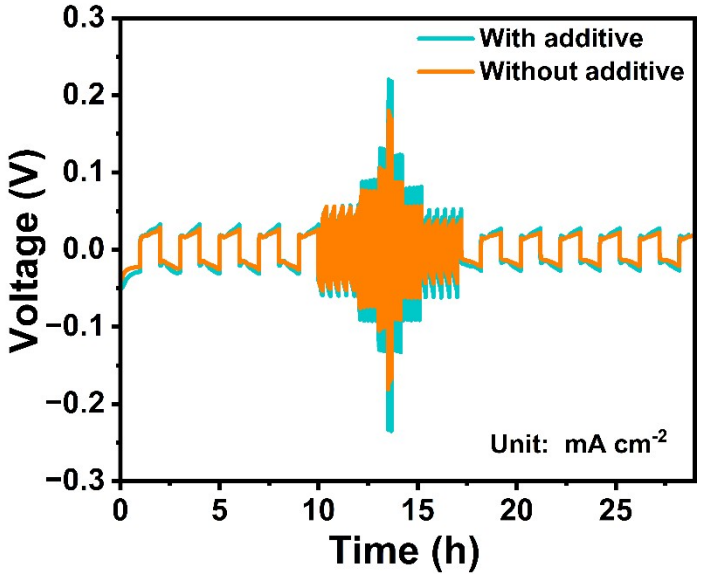

Figure S13. Rate performance of Zn-Zn symmetric batteries with and without the BA additives at current densities of 1, 5, 10, 20, and 50 mA cm^{-2} with a capacity of 1 mAh cm^{-2}.

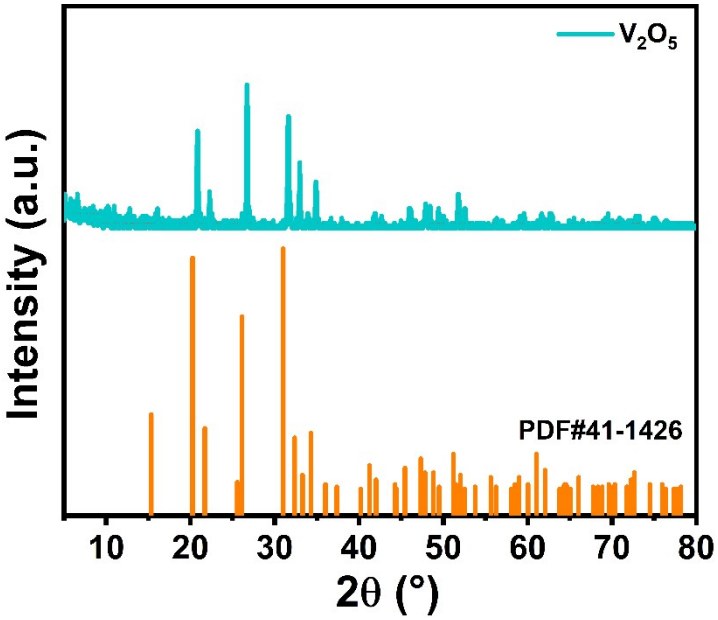

Figure S14. XRD spectrum of V_2O_5.

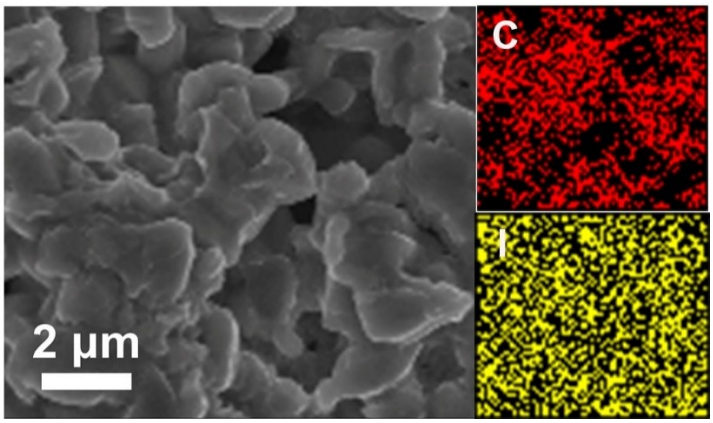

Figure S15. SEM image and EDS mapping of I_2-based materials.

Table S1. Comparison of current density and cycling life of Zn anodes.

Electrode material	Electrolyte	Current density (mA cm^{-2})	Lifetime (h)	Ref.
Cu and Zn sites anchored on N,P-codoped carbon macroporous fibers	2 M $ZnSO_4$	2	630	[9]
Zn@Cu(111)	2 M $ZnSO_4$	5	62.5	[10]
Zn	10 mM 7,7,8,8-tetracyanoquinodimethane modified 2 M $ZnSO_4$	1	1200	[11]

Zn	3 M $ZnSO_4$ with 5 mM hexamethylenetetramine	5	590	[12]
Zn	1 M $ZnSO_4$ with 2 wt% polydiallyl dimethylammonium chloride	1	3000	[13]
Laponite film@Zn	2 M $ZnSO_4$	0.5	1100	[14]
Ethylenediaminetetraacetic acid functionalized MOF-808	2 M $ZnSO_4$	2	900	[15]
Stearic acid@Zn	2 M $ZnSO_4$	1	2000	[16]
Zn	2 M $Zn(CF_3SO_3)_2$ with 5 wt % methylammonium acetate	0.5	1800	[17]
Zn-HfO_2	2 M $ZnSO_4$	1	1400	[18]
Zn	0.5 M $Zn(CF_3SO_3)_2$-NMF	3	400	[19]
Zn	3 M $Zn(CF_3SO_3)_2$ and 0.1 M ZnI_2 in 90% EG/H_2O	5	300	[20]
Zn	KevlarH electrolyte	1	3500	[21]
Zn	2 M $ZnSO_4$ with 1 vol. % pyridine	5	500	[22]
Zn	2 M $ZnSO_4$ with 5 wt % butyrolactam	0.5 1 2 5 10 20	6200 3900 2000 968 800 190	This work

REFERENCES

[1] Q. Guo, H. Wang, X. Sun, Y. Yang, N. Chen, L. Qu, *ACS Materials Lett.*, 2022, **4**,1872−1881.

[2] G. Kresse, J. Furthmüller, *Comp. Mater. Sci.*, 1996, **6**, 15-50.

[3] J. P. Perdew, K. Burke, M. Ernzerhof, *Phys. Rev. Lett.*, 1996, **77**, 3865-3868.

[4] G. Henkelman, H. Jónsson, *J. Chem. Phys.*, 2000, **113**, 9978-9985.

[5] S. Plimpton, *J. Comput. Phys.*, 1995, **117**, 1-19.

[6] H. J. C. Berendsen, J. R. Grigera, T. P. Straatsma, *J. Phys. Chem.*, 1987, **91**, 6269-6271.

[7] E. Clementi, G. Corongiu, B. Jönsson, S. Romano, *J. Chem. Phys.*, 1980, 72, 260-263.

[8] I. M. Zerón, J. L. F. Abascal, C. Vega, *J. Chem. Phys.*, 2019, 151, 134504.

[9] Y. Zeng, Z. Pei, D. Luan, X. Lou, *J. Am. Chem. Soc.*, 2023, **145**, 12333–12341.

[10] Y. Su, B. Chen, Y. Sun, Z. Xue, Y. Zou, D. Yang, L. Sun, X. Yang, C. Li, Y. Yang, X. Song, W. Guo, S. Dou, D. Chao, Z. Liu, J. Sun, *Adv. Mater.*, 2023, **35**, 2301410.

[11] P. Xiong, C. Lin, Y. Wei, J.-H. Kim, G. Jang, K. Dai, L. Zeng, S. Huang, S. J. Kwon, S.-Y. Lee, H. S. Park, *ACS Energy Lett.*, 2023, **8**, 2718−2727.

[12] H. Yu, D. Chen, Q. Li, C. Yan, Z. Jiang, L. Zhou, W. Wei, J. Ma, X. Ji, Y. Chen, L. Chen, *Adv. Energy Mater.*, 2023, **13**, 2300550.

[13] M. Peng, X. Tang, K. Xiao, T. Hu, K. Yuan, Y. Chen, *Angew. Chem. Int. Ed.*, 2023, **62**, e202302701.

[14] J. Feng, X. Li, X. Cui, H. Zhao, K. Xi, S. Ding, *Adv. Energy Mater.*, 2023, **13**, 2204092.

[15] R. Zhang, Y. Feng, Y. Ni, B. Zhong, M. Peng, T. Sun, S. Chen, H. Wang, Z. Tao, K. Zhang, *Angew. Chem. Int. Ed.*, 2023, **62**, e202304503.

[16] M. Fu, H. Yu, S. Huang, Q. Li, B. Qu, L. Zhou, G.-C. Kuang, Y. Chen, L. Chen, *Nano Lett.*, 2023, **23**, 3573–3581.

[17] L. Zheng, H. Li, X. Wang, Z. Chen, C. Hu, K. Wang, G. Guo, S. Passerini, H. Zhang, *ACS Energy Lett.*, 2023, **8**, 2086−2096.

[18] J.-L. Yang, L. Liu, Z. Yu, P. Chen, J. Li, P. A. Dananjaya, E. K. Koh, W. S. Lew, K. Liu, P. Yang, H. J. Fan, *ACS Energy Lett.*, 2023, **8**, 2042−2050.

[19] B. Raza, Y. Zhang, J. Chen, U. Shamraiz, Y. Zhang, A. Naveed, J. Wang, *Angew. Chem. Int. Ed.*, 2023, **62**, e202302174.

[20] Y. Yang, S. Guo, Y. Pan, B. Lu, S. Liang, J. Zhou, *Energy Environ. Sci.*, 2023,**16**, 2358-2367.

[21] Y. Yang, H. Hua, Z. Lv, W. Meng, M. Zhang, H. Li, P. Lin, J. Yang, G. Chen, Y. Kang, Z. Wen, J. Zhao, C. C. Li, *ACS Energy Lett.*, 2023, **8**, 1959−1968.

[22] J. Luo, L. Xu, Y. Zhou, T. Yan, Y. Shao, D. Yang, L. Zhang, Z. Xia, T. Wang, L. Zhang, T. Cheng, Y. Shao, *Angew. Chem. Int. Ed.*, 2023, **62**, e202302302.